

On the Accuracy of Current Measurements by Means of HF Radar

Heinz-Herman Essen, Klaus-Werner Gurgel, *Member, IEEE*, and Thomas Schlick

Abstract—The accuracy of surface current velocities measured by high-frequency (HF) radar is investigated. Data from the two radar systems of the University of Hamburg, CODAR (Coastal Radar) and WERA (Wellen Radar), are compared with *in situ* data. In one experiment, CODAR and a near-surface current meter were operated simultaneously over a 19-day period. In addition, WERA was operated for 6 days during that period. In the other experiment, WERA and a bottom-mounted current meter were operated simultaneously over a 35-day period. Both radars use frequencies of about 30 MHz where backscattering is due to ocean waves of 5 m wavelength. The influence of the orbital motion of underlying longer waves on radial velocity errors is investigated. In accordance with theory, the measured standard deviations of HF-measured current velocities depend on the sea state. Depending on the sea state, estimated errors range from 3 to 10 $\text{cm}\cdot\text{s}^{-1}$ and explain only part of the rms difference of 10–20 $\text{cm}\cdot\text{s}^{-1}$ found between HF and *in situ* current measurements. The rest is assumed to be due the differences of the quantities measured, e.g., the spatial averaging.

Index Terms—Error statistics, HF radar, surface current.

I. INTRODUCTION

HIGH-FREQUENCY (HF) radars allow one to map surface currents off shore by means of land-based stations. The Doppler shift of the backscattered signal is used for measuring the radial current speed relative to the radar site. Guided propagation along the conductive sea surface (ground wave) allows measurements beyond the horizon. The basic physics of backscattering of electromagnetic waves from a rough sea surface was discovered by Crombie in 1955 [1].

In 1977, Barrick *et al.* [2] developed the first HF radar capable of measuring surface currents, the Coastal Radar (CODAR), originally called Coastal Ocean Dynamics Application Radar. Based on CODAR, developments have been performed in the United Kingdom with the Ocean Surface Current Radar (OSCR) (Prandle [3]), in Germany [4], and in the United States with the SeaSonde [5]. Developments independent of CODAR have been made in Canada [6], in the UK [7], France [8], Australia [9], Japan [10], and in the United States by the Stanford group [11]. More detailed information on these systems is given by Gurgel *et al.* [12].

HF radars allow the measurement of surface currents which, due to the contamination by surface waves, are hard to obtain by moored current meters. HF-measured currents are available as a

surface map on a regular grid. Such data are needed for the interpretation of surface structures visible in satellite images. Essen [13] related a field of sea-surface temperature (SST) to surface currents measured by CODAR. Another example of this application is the work of Graber *et al.* [14]. The authors compare current velocities extracted from Interferometric Synthetic Aperture Radar (INSAR) data and measured by the HF radar OSCR.

Surface current fields as measured by HF radar can be used to verify numerical circulation models or to improve, by assimilation methods, their results. The European Radar Ocean Sensing (EuroROSE) project, funded by the European Union, aims at predicting, for a few hours, off-shore currents in coastal areas of high ship traffic. For this purpose, HF-measured surface current velocities will be assimilated by a three-dimensional (3-D) numerical model. In addition to the current velocities, the assimilation scheme requires knowledge of the error statistics. Estimation of the errors is the objective of this paper.

Several comparisons of current velocities measured by HF radars and by conventional means are reported in the literature. The rms differences between the two components of the horizontal current velocity vary between 10 cm^{-1} and 20 cm^{-1} , cf. [11] and [15]. However, HF radars and conventional instruments measure different quantities. HF radars (of transmit frequency around 30 MHz) average over an area of a few km^2 and over the upper 50 cm of the ocean, while conventional instruments perform point measurements. Mostly, *in situ* measurements are carried out only for a depth of a few meters below the surface or more and observe reduced wind drift and Stokes drift. Additional evidence for the accuracy of HF measured current velocities has been obtained by analyzing time series. The HF measured current velocity shows a strong correlation with the wind vector, cf. [16], and reasonable tidal portions, cf. [3].

Current speed is retrieved from the Doppler shift of the backscattered HF signal. The achievable accuracy depends on the temporal and spatial resolution (uncertainty relation). The determination of current speed relies on the linear dispersion relation for surface waves, although ocean waves are (weakly) nonlinear. These effects are discussed shortly. More emphasis is put on the influence of long waves which carry the short scattering Bragg waves (wavelength of 5 m for a 30-MHz radar).

Data from two experiments are presented. HF and conventional current measurements are compared. During both experiments, a directional waverider was deployed in the area covered by the HF measurements. The measured wave spectra are used to predict the standard deviation of the HF measurements. A strong dependence on sea state for both theory and measurement is found. However, the comparison shows that the theory overestimates the observed standard deviation.

Manuscript received August 24, 1999; revised August 23, 2000. This work is part of the EuroROSE-project, supported by the European Union (EU). The *in situ* data used were gathered during the SCAWVEX experiments (funded by EU) by Rijkswaterstaat and Proudman Oceanographic Laboratory.

The authors are with the Institut für Meereskunde der Universität Hamburg, 22529 Hamburg, Germany.

Publisher Item Identifier S 0364-9059(00)11468-2.

II. THEORY

A CW HF radar is characterized by its carrier (circular) frequency ω_0 and its wavevector \mathbf{k}_0 which is parallel to the sea surface, i.e., two-dimensional (2-D). Part of the transmitted energy is backscattered by ocean surface waves.

Ocean surface waves are assumed to be a homogeneous random process. They are described by the directional (2-D) waveheight spectrum F

$$F(\mathbf{k}) = \frac{1}{k} E(k) S(k, \varphi) \quad (1)$$

where $\mathbf{k} = (k \sin \varphi, k \cos \varphi)$ is the wavevector and φ the wave direction. The wavenumber k and the circular frequency ω of ocean waves are connected by the deep-water dispersion relation. E is the one-dimensional wavenumber spectrum and S is the (normalized) directional distribution.

A. Bragg Scattering

Backscattering is well described by Bragg theory. To first order, the backscatter is due to ocean waves of half of the radar wavelength travelling toward or away from the radar site (Bragg waves):

$$\mathbf{k}_B = \mp 2\mathbf{k}_0. \quad (2)$$

The moving Bragg waves induce a Doppler shift to the backscattered HF signal

$$\omega_d = \pm \omega_B - 2\mathbf{k}_0 \mathbf{u} \quad (3)$$

where the sign of ω_B is determined by the direction of the scattering Bragg wave and the magnitude by k_B through the dispersion relation. The first term is due to the phase velocity of the scattering Bragg waves and the second term due to underlying currents \mathbf{u} . Equation (3) is the basis for HF radar measurement of the radial component of surface currents.

First-order Bragg theory predicts a Doppler spectrum consisting of two discrete lines. Second-order contributions are continuous. In the case that the main variance of the ocean waveheight spectrum is concentrated at wavelengths which are much longer than the Bragg wave, the second-order Doppler spectrum becomes (cf. [17])

$$D(\omega_D) = F(\mathbf{k}_B) \int T(K, \varphi) E(K) S(K, \varphi) d\varphi, \\ \omega_D = \pm \omega_B \pm \Omega, \quad \Omega^2 = gK \quad (4)$$

where K and Ω denote wavenumber and circular frequency of the long surface waves. T is a theoretically known transfer function and g the gravity acceleration. Thus, two second-order Doppler spectra fold around both Doppler lines. Among others, Wyatt [18] uses (4) for retrieving ocean-wave spectra by means of inversion methods.

B. Composite Wave Model

The Bragg theory assumes that surface currents are stationary during the measurement time of, e.g., 10 min. However, orbital motions of long waves (carrying the short Bragg waves) induce

a Doppler shift which varies during the measuring time. These waves cause a broadening of the first-order Doppler spectrum. The effect is estimated by means of the composite wave model, cf. Wright [19]. The model assumes that the wavelengths of the modulating surface waves are much longer than those of the scattering Bragg waves. The long waves are locally approximated by plane facets. The facets move with the orbital motion of the long waves. Our approach does not account for the slopes of the facets (tilt modulation).

The HF measurements perform both averaging in space (due to the pulse length) and time (due to the measuring time). The orbital velocity can be considered as a random variable with zero mean and normal probability distribution. Because of the linear dependence on the orbital velocity (3), ω_d is normally distributed with mean m and variance σ^2 as

$$m = \langle \omega_d \rangle = \pm \omega_B - 2k_0 U_x, \\ \sigma^2 = \langle (\omega_d - m)^2 \rangle = 4k_0^2 \langle u_x^2 \rangle \quad (5)$$

where, for simplicity, it is assumed that the radar wavevector \mathbf{k}_0 points along the direction of the x axis. U_x is the radial component of the underlying homogeneous and stationary current, and u_x is the radial component of the orbital motion of the long ocean waves.

Linear ocean-wave theory determines the variance of the orbital velocity component u_x in terms of the 2-D waveheight spectrum

$$\langle u_x^2 \rangle = g \int \frac{K_x^2}{K} F(\mathbf{K}) d\mathbf{K} \quad (6)$$

where the capital \mathbf{K} indicates that the integration refers to the modulating long waves.

Two model spectra, often used in the literature, are discussed with respect to their influence on the broadening of the Doppler spectrum. The spectra under consideration can be represented as

$$E(K) = \frac{A}{K^3} \exp \left[-1.25 \left(\frac{\Omega}{\Omega_p} \right)^{-4} \right] e(\Omega) \quad (7)$$

where Ω_p is the peak frequency of the frequency spectrum and $e(\Omega)$ is the peak enhancement factor.

In 1964, Pierson and Moskowitz [20] proposed a spectrum for a fully developed sea

$$A = 0.005, \quad \Omega_p = 0.88 \frac{g}{U}, \quad e(\Omega) = 1. \quad (8)$$

Based on measurements, Hasselmann *et al.* [21] modified the Pierson–Moskowitz spectrum by describing both the amplitude A and peak frequency Ω_p in (7) in terms of a nondimensional fetch and by introducing the peak enhancement factor. A typical JONSWAP spectrum is given by

$$A = 0.038 \tilde{x}, \quad \Omega_p = \frac{22g}{U} \tilde{x}^{-0.33}, \quad e(\Omega) = 3.0^\beta, \\ \beta = \exp \left[-0.5 \left(\frac{\Omega - \Omega_p}{s\Omega_p} \right)^2 \right], \quad s = \begin{cases} 0.08, & \text{if } \Omega \leq \Omega_p, \\ 0.12, & \text{if } \Omega > \Omega_p \end{cases} \quad (9)$$

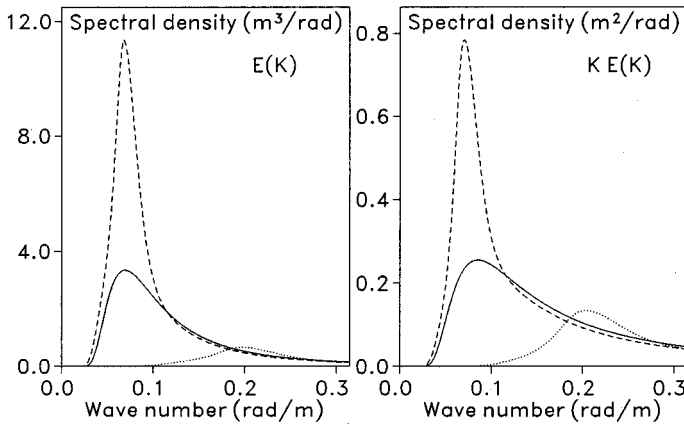


Fig. 1. Long-wave spectra of waveheight $E(K)$ (left panel) and the quantity $KE(K)$ (right panel), Pierson-Moskowitz (full lines), JONSWAP with long fetch (dashed lines) and short fetch (dotted lines), cf. (7)–(9). The wind speed is 10 ms^{-1} .

where $\tilde{x} = gx/U^2$ is the nondimensional fetch and x the fetch measured in meters.

Fig. 1 displays wavenumber spectra of the waveheight $E(K)$ and the quantity $KE(K)$ which determines the Doppler broadening, cf. (6). A wind speed of 10 ms^{-1} and two different fetches are considered. Linear scales have been chosen in order to clarify the differences of variances. The long fetch ($\tilde{x} = 2 \times 10^4$, $\tilde{u} = 0.84$) refers to a fully developed sea. Decreasing the fetch by a factor of five, the waveheight spectra contain considerably less variance.

The directional distribution is assumed to be

$$S(k, \varphi) = \begin{cases} 0.64 \cos^2(\varphi - \phi), & \text{if } |\varphi - \phi| \leq 90^\circ, \\ 0, & \text{otherwise} \end{cases} \quad (10)$$

where ϕ is the mean wind direction.

Table I represents standard deviations of the radial current speed calculated by means of (6) for the spectra presented. There is a strong dependence on sea state, characterized by wind speed and direction. It should be mentioned that the results depend on the cutoff wavenumber chosen.

C. Other Error Sources

Other (minor) errors are induced by the finite length of the measurement, the limited extent of the scattering area, and the nonlinearity of the dispersion relation.

For a 30-MHz radar, the measuring time of 10 min allows to resolve the radial speed with $1 \text{ cm}\cdot\text{s}^{-1}$ (Fourier decomposition). The limited extent of a scattering area implies a wavenumber broadening of the backscattered wavenumber (uncertainty relation). The scattering area is defined by the pulse length or, in the facet model, by the (smaller) facet size. In the facet model, the average uncertainty has to be considered. Both methods result in an error of less than $1 \text{ cm}\cdot\text{s}^{-1}$. Considering a facet diameter of $L = 10\lambda_B$ (wavelength of the Bragg wave), the uncertainty of the wavenumber becomes $\Delta k \approx 1/L \approx 0.02k$ and that of the radial speed $\Delta U \approx 3 \text{ cm}\cdot\text{s}^{-1}$. Averaging over 10 facets results in the error stated.

The dispersion relation of ocean waves is needed to determine the phase velocity of the scattering Bragg waves which is

TABLE I
THEORETICAL STANDARD DEVIATION OF RADIAL CURRENT SPEED [$\text{cm}\cdot\text{s}^{-1}$] DUE TO THE PRESENCE OF LONG WAVES. RESULTS ARE PRESENTED FOR DIFFERENT WIND SPEEDS U AND WIND DIRECTIONS PARALLEL AND PERPENDICULAR TO THE RADAR BEAM. LONG-WAVE SPECTRA USED ARE: A) PIERSON-MOSKOWITZ, B) JONSWAP (LONG FETCH), AND C) JONSWAP (SHORT FETCH), Cf. FIG. 1. THE CUTOFF WAVELENGTH IS 20 m

U [ms^{-1}]	parallel			perpendicular		
	A	B	C	A	B	C
5	11	18	0	6	11	0
10	52	61	17	30	36	10
15	82	88	48	47	51	28

the reference for the calculation of the current speed. The dispersion relation used is based on linear wave theory. The nonlinear correction depends on the wave slope, cf. Kinsman [22]. Considering, in accordance with the uncertainty relation for the facet model, a wavenumber interval of $\pm 0.02k$, the spectra of the previous chapter yield standard deviations of the slope of less than 0.03 (independent of wind speed). Inserting into the nonlinear dispersion relation, the phase-velocity error becomes $0.2 \text{ cm}\cdot\text{s}^{-1}$.

III. HF RADARS

In 1980, the University of Hamburg adopted the Coastal Radar (CODAR) of NOAA [2]. Both hardware and software had been modified in order to increase sensitivity and optimize processing algorithms. Since 1985, the CODAR has been operated in 15 field experiments, e.g., [23], [24], and from onboard a ship [25]. It should be mentioned that the CODAR under consideration is not the CODAR SeaSonde [5]. Progress in electronics and computer techniques have allowed the design of a new system called Wellen Radar (WERA), cf. Gurgel *et al.* [26]. Both CODAR and WERA use transmit frequencies between 25 and 30 MHz. The polarization is vertical for both transmitting and receiving. The low-gain transmit antenna is directed toward the sea. Azimuthal resolution is performed by means of an array of receive antennas, and range resolution via the travel time, either by pulse or chirp techniques.

A. CODAR

The CODAR used [4] transmits CW pulses. The length of the tapered pulse determines the range resolution which is about 2 km. Range sampling is 1.2 km. Azimuthal resolution is performed by means of a four-element square array of receive antennas. The backscattered signal is phase-coherently demodulated and sorted into range cells. The resulting (slowly-varying) time series are Fourier transformed. Fourier lines with amplitudes exceeding a certain threshold are analyzed. The frequency offset relative to the two Bragg lines determines the radial current speed. The intercomparison of the phases at the four receive antennas yields the azimuthal angle of arrival (direction finding). The main advantage of the CODAR is the small size of the antenna array which can be deployed nearly anywhere. The main disadvantage is that direction finding can be distorted by ambiguities.

For the experiments presented, the CODAR carrier frequency was 29.85 MHz. The sampling rate of the demodulated time

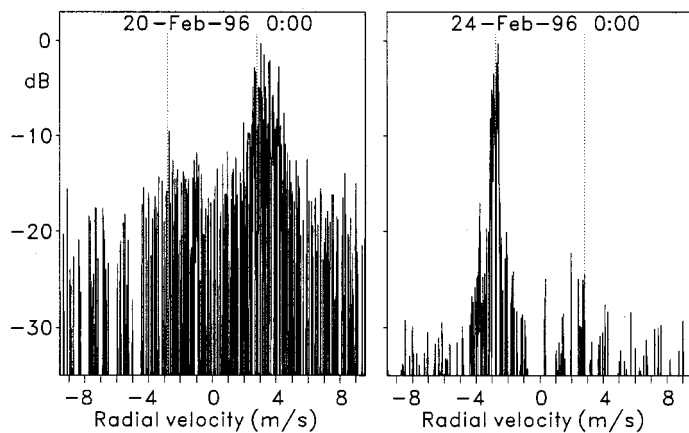


Fig. 2. CODAR Doppler spectra received from an area of about 3×3 km at a distance of 15 km from the radar site, during high sea state (left) and low sea state (right). The dB-scale refers to the maximum spectral line. Vertical dotted lines represent the Bragg phase velocities $\pm\omega_B/k_B$.

series was 0.262 s and the number of samples 4096 (≈ 18 min). It has been found that subdividing the full (18 min) time series into seven subseries with 50% overlap produces more robust results than processing the full series. This method yields a resolution of $1.9 \text{ cm}\cdot\text{s}^{-1}$ for the radial velocity. However, the averaging of several spectral lines can provide a higher accuracy.

Fig. 2 displays CODAR Doppler spectra in terms of the radial velocity which is related to frequency by (3). Direction finding has been applied. The Doppler lines presented are from two adjacent range cells and an azimuthal angular interval of 12° . The left spectrum has been observed at high sea state with the significant waveheight exceeding 4 m, while the significant waveheight was less than 0.5 m for the right spectrum. The examples demonstrate the general behavior that the Doppler spectrum becomes broader and the noise level increases with increasing sea state.

B. WERA

One advantage of WERA is the flexibility in range resolution between 0.3 and 1.2 km. This is achieved by transmitting Frequency-Modulated Continuous Wave (FMCW) chirps. In addition, this technique avoids the blind range of about 3 km in front of the CODAR. A further advantage of WERA is the possibility of connecting up to 16 receive antennas. When operating with a linear array, beamforming in the time domain is used for azimuthal resolution. Fourier analysis of the beam time-series yields the Doppler spectrum for a resolution cell on the sea surface, defined by the width of the range cell and the width of the beam. The peak frequency of the Doppler spectrum determines the current speed, and the broadness of the spectrum allows one to estimate the standard deviation of the current speed. Second-order side bands can be separated and used to retrieve information on the sea state.

During the experiments presented, the WERA carrier frequency was either 29.85 or 27.65 MHz, the sampling interval 0.26 s, and the number of samples 2048 (≈ 9 min). Again the time series were subdivided into seven overlapping subseries which yield a resolution in the radial velocity of about $4 \text{ cm}\cdot\text{s}^{-1}$. Fig. 3 shows WERA Doppler spectra. The surface area illu-

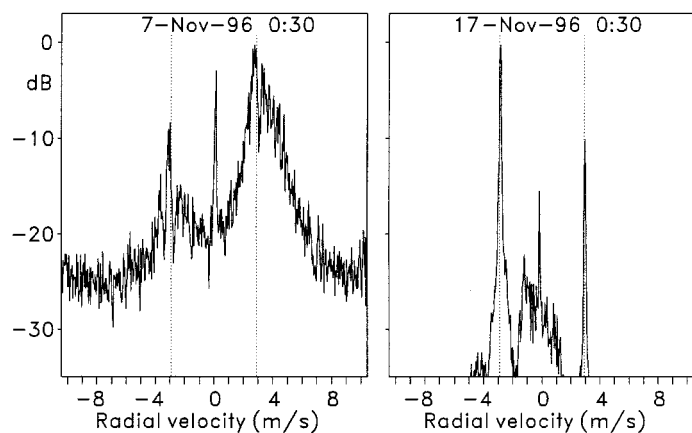


Fig. 3. WERA Doppler spectra received from an area of about 3×3 km at a distance of 15 km from the radar site, during high sea state (left) and low sea state (right). The dB-scale refers to the maximum spectral line. Vertical dotted lines represent the Bragg phase velocities $\pm\omega_B/k_B$.

minated and the sea states considered (significant waveheights of 4 m and 1 m for the left and right panel, respectively) are about the same as for the CODAR spectra of Fig. 2. Again, the broadness of the Doppler spectrum and the noise level depend on the sea state. However, the WERA Doppler spectra seem to allow a more precise determination of the peak than the CODAR spectra.

IV. EXPERIMENTAL DATA

The data used in this paper are from the Surface Current and Wave Variability Experiments (SCAWVEX), performed off the Dutch coast in February/March 1996 (Maasmond experiment) and in November/December 1996 (Petten experiment). Fig. 4 shows the Dutch coast and the locations of the sensors referred to in this paper. For both experiments, we compare HF and *in situ* current measurements. Then, the spectra measured by the directional waverider are used to predict theoretically the standard deviation of the HF-measured current velocities. The results are compared with the measured standard deviations. These are used to estimate the errors.

A. Maasmond Experiment

The aim of the Maasmond experiment was to measure current velocities. Two HF sites were set up south and north of the Rhine mouth. Both the CODAR and WERA systems were deployed in order to check proper operation of the new WERA and to compare different methods for azimuthal resolution. A comparison of the performance of both systems is given by Gurgel *et al.* [26]. The conclusion is that direction-finding with a four-element square array (CODAR) basically gives the same measurements of radial speeds as beamforming with a 12-element linear array (WERA). However, the data processed with direction-finding seems to be more noisy in the area of high ship traffic. Fig. 5 shows a typical current map as measured by CODAR.

In situ measurements, as listed in Table II, were carried out at the sites indicated in Fig. 4. The directional waverider was operated by Rijkswaterstaat. Wind data are available from a po-

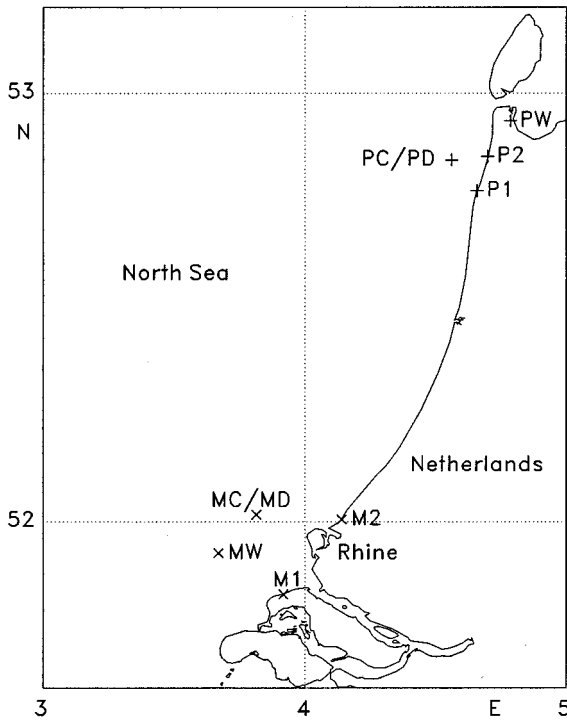


Fig. 4. Dutch coast and measuring sites during the Maasmond experiment (southern part) and the Petten experiment (northern part). The two radar sites of the Maasmond experiment are M1 and M2 and those of the Petten experiment P1 and P2. Positions of current meters (MC/PC), directional waveriders (MD/PD), and wind sensors (MW/PW) are indicated accordingly.

sition close to the waverider and current-meter moorings. The wind time series starts on March 1, i.e., later than the current and wave measurements. The WERA was operational only during the last eight days of the experiment.

Fig. 6 compares the CODAR measurements with data of an electromagnetic current meter (S4), deployed 1 m below the sea surface. The S4 (InterOcean systems, Inc.) measures the voltage resulting from the motion of the conductive water through a magnetic field. The CODAR radial speeds are averages over 3 range cells and an azimuthal section of 9° . This results in an area extending 3.6 km in range and 3.4 km in azimuth around the position of the current meter (position MC in Fig. 4). The overall rms differences between the radial components u_1 and u_2 of the CODAR and S4 measurements are 18 and 21 $\text{cm}\cdot\text{s}^{-1}$, respectively. The respective correlation coefficient are both $r = 0.91$. Some single days reveal much better agreement, e.g., March 10 with rms differences of 8 and 9 $\text{cm}\cdot\text{s}^{-1}$ of the two radial components.

The difference between the current vectors, measured by CODAR and by S4, is displayed in Fig. 7 and compared with the wind vector. The complex correlation coefficient $R = \rho \exp(i\alpha)$ (vector correlation, cf. Kundu [27]) quantitatively describes the relation between the vector time series of the difference velocity and wind. α is the average veering between the vector series and ρ^2 describes the portion of variance explained by the linear dependence of the time series. The correlation between the series of Fig. 7 is $\rho = 0.41$ and $\alpha = 4^\circ$ which is the veering of the current difference from the wind to the right.

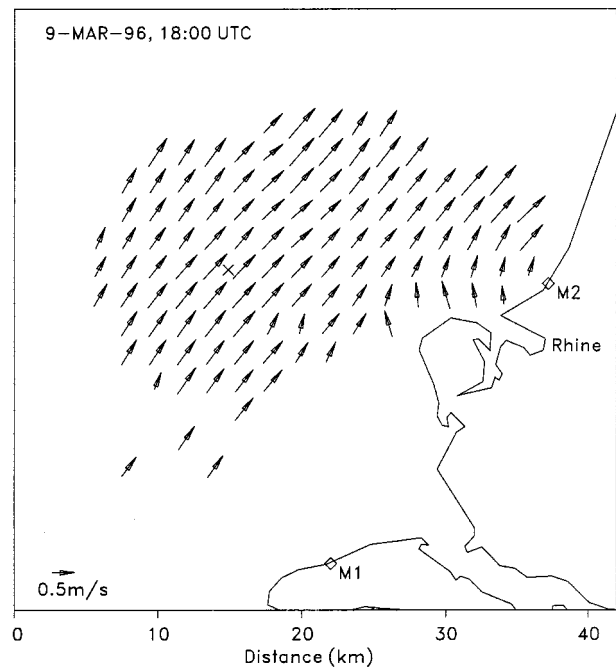


Fig. 5. Map of surface current velocity as measured by CODAR. Arrows point into the direction of the current, and the length is proportional to the speed. Position MC of Fig. 4 is marked by a cross.

TABLE II
MEASUREMENTS DURING THE SCAWVEX MAASMOND EXPERIMENT

site	parameter	sensor	period
M1	radial current	CODAR	18 Feb - 26 Mar
M1	radial current	WERA	18 Mar - 26 Mar
M2	radial current	CODAR	18 Feb - 26 Mar
M2	radial current	WERA	18 Mar - 26 Mar
MC	current vector	S4	23 Feb - 24 Mar
MD	wave spectra	waverider	18 Feb - 26 Mar
MW	wind vector	windsensor	1 Mar - 18 Mar

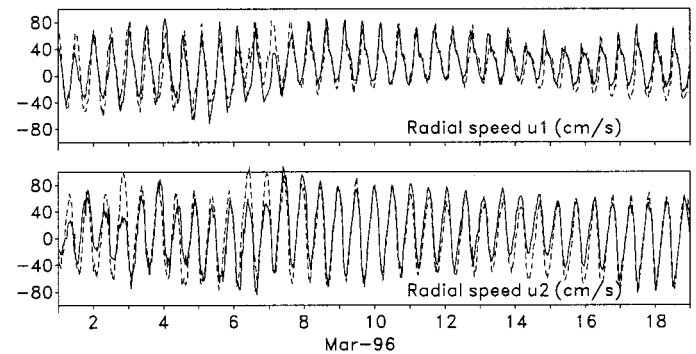


Fig. 6. Comparison of radial speeds u_1 and u_2 measured by CODAR sites M1 and M2 in Fig. 4, respectively (full lines), with the projections of the S4-current measurements onto these components (dashed lines). The sampling interval is 1/2 h.

There are several possible candidates for the rms difference between the two current measurements. One is the fact that the near-surface CODAR measurements (effective depth ≈ 20 cm) are more affected by wind and Stokes drift than the S4 measurements 1 m below the sea surface. However, most of the rms

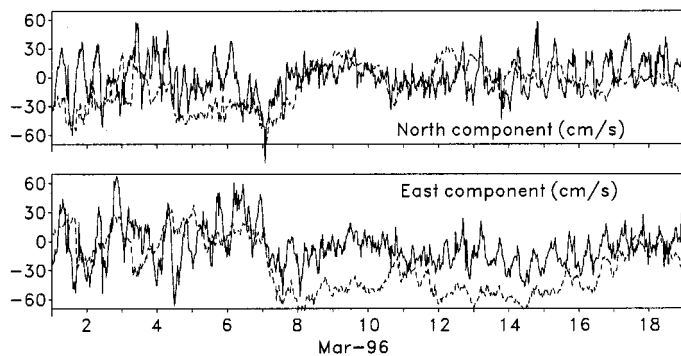


Fig. 7. Difference of the current vectors CODAR-S4 (full lines) and wind vector multiplied by a factor of 0.02 (dashed lines), both displayed as north- and east-components.

difference is due to some events where the S4 measures higher tidal amplitudes than the CODAR and occasional phase shifts between the tides of the order of 1 h. We suspect that some portion of the rms difference is due to horizontal averaging performed by the CODAR in contrast to the point measurement of the S4. The experimental area is influenced by the Rhine outflow which causes current shears both horizontal and vertical.

For the period March 18, 0:00, until March 24, 9:00, UTC current measurements were performed simultaneously by the HF systems CODAR and WERA and by the *in situ* instrument S4. During this period, the significant waveheight was below 1 m. RMS differences of the current measurements are presented in Table III. The WERA reveals somewhat better agreement with the S4 than the CODAR.

CODAR and WERA measurements have been performed successively with measuring periods of 18 min and 9 min, respectively. The different temporal averaging and the interpolation onto a common time base may explain some of the rms differences. However, most of the deviation must be attributed to measuring errors. The rms difference between CODAR and WERA current measurements increases from values less than 5 cm·s⁻¹ at ranges below 10 km to values higher than 10 cm·s⁻¹ at ranges above 20 km. Somewhat increased rms differences are found in areas with heavy ship traffic. From investigating the data, we conclude that the CODAR is, with respect to perturbations by ship traffic, less robust than the WERA, cf. [26].

In order to estimate the error of the CODAR measurement, we make use of the spectra measured by the directional waverider, deployed at the same position as the S4 current meter, cf. Fig. 4. The directional waverider measures the one-dimensional waveheight spectrum in terms of frequency and for each frequency point the mean direction and the directional spreading. Fig. 8 shows a spectrum, transformed to wavenumber, i.e., the dimensions are the same as those in Fig. 1. The spectrum is from February 20 when the sea state reached the maximum of the measuring campaign with significant waveheights exceeding 4 m for about one day.

Fig. 9 displays measured wavespectra, theoretically predicted, and measured standard deviations and estimated errors of the CODAR surface-current measurements. A waveheight vector is derived from the significant waveheight and the direction at the spectral peak. The components of this vector

TABLE III
RMS DIFFERENCES [cm·s⁻¹] AND CORRELATION COEFFICIENT (IN BRACKETS) FOR TWO OF THE THREE TIME SERIES, CODAR (CO), WERA (WE), AND S4. THE TIME SERIES OF 300 DATA ARE SAMPLED EVERY HALF HOUR

	CO-S4	WE-S4	CO-WE
u1	14 (0.89)	11 (0.93)	9 (0.96)
u2	15 (0.96)	13 (0.97)	11 (0.98)

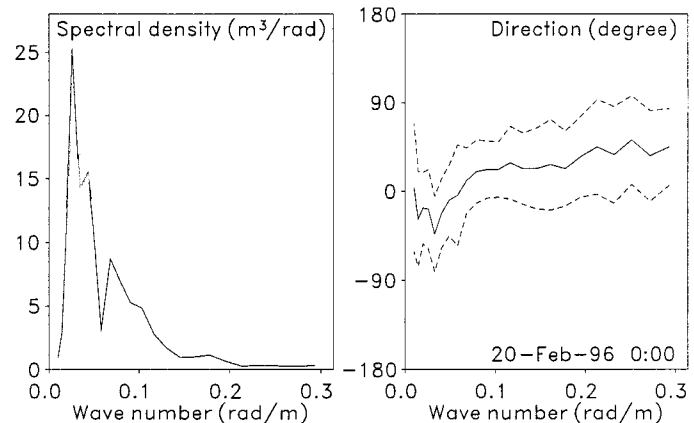


Fig. 8. Waveheight spectrum measured by the directional waverider buoy. The left panel displays the one-dimensional wavenumber spectrum, and the right panel the mean direction (full lines) and the directional spreading (dashed lines).

parallel to the directions of the radial velocities u_1 and u_2 are shown in the upper panel of Fig. 9. The absolute values of these components are displayed, because waves of opposite direction yield the same contribution to the standard deviation. The period February 19–27 was selected, as it contains both high and low sea states. During the following three weeks of the experiment, the sea state was moderate.

The theoretical standard deviations in Fig. 9 have been computed by means of (6) using the measured waveheight spectra. Their directional distribution is assumed to be Gaussian with the broadness determined by the measured spreading. The theoretical standard deviation reveals a strong dependence on the sea state.

CODAR-measured (mean) radial speed is determined from the frequencies of a number of Doppler lines which exceed a certain threshold. Averaging is performed by weighting with the signal strength (squared amplitude of a Doppler line) and yields both the radial speed (mean) and its standard deviation. There is a high correlation of $r = 0.86$ between the waveheight component (upper panel of Fig. 9) and the standard deviation (third panel of Fig. 9) of station M1 and a lower correlation of $r = 0.46$ of station M2. This difference may be explained by the different amplitudes of the waveheight components.

For the period of high sea states, February 19–21, the CODAR standard deviation increases. This is in accordance with the theory. However, the values are about only one half of the predicted ones. One reason for this finding is that the CODAR variance depends on the weighting applied. The variance increases by using the amplitude instead of the signal strength (squared amplitude) which, however, is disadvantageous for the determination of the peak frequency. Another reason may be that the requirements for the composite wave

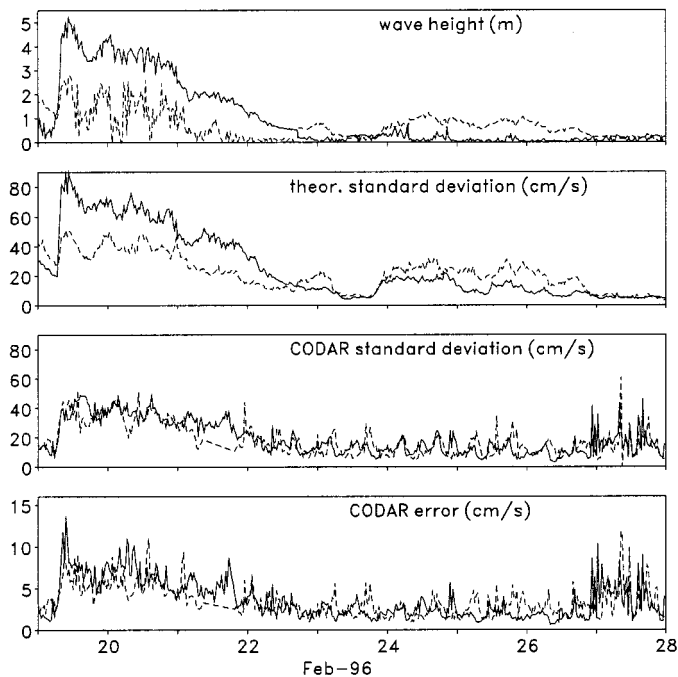


Fig. 9. Upper panel: significant waveheight measured at MD in Fig. 4, parallel to the direction toward M1 (full line) and M2 (dashed line). Second panel: theoretically predicted standard deviations for the radial speeds of stations M1 (full line) and M2 (dashed line). Third panel: standard deviations measured by CODAR stations M1 (full line) and M2 (dashed line) at position MD. Bottom lower panel: CODAR error derived from the standard deviation.

model are violated. The long waves involved are too short, in relation to the Bragg wavelength, for being approximated by plane facets.

The bottom panel of Fig. 9 displays the estimated errors of the CODAR measurements. These are derived from the standard deviations by dividing by the square root of the number of independent measurements. This value is assumed to be the sum of the Doppler lines used, each weighted by its signal strength. Especially during February 27, the CODAR standard deviation and in turn the error shows a number of single peaks. One possible cause is the low sea state which results in low backscatter. Reduced backscatter strength does not necessarily produce higher errors, but it reduces the signal-to-noise ratio and, in turn, the range. The measurements are more easily disturbed, e.g., by radio interference or ship traffic.

B. Petten Experiment

The main aim of the Petten experiment was to demonstrate the capability of WERA for measuring waves. The area was chosen by Rijkswaterstaat who has been operating a transect of wave measuring buoys, extending from 7 km offshore up to the dike between positions P1 and P2 in Fig. 4. Additional measuring systems were included for the period of the SCAWVEX experiment, cf. Table IV. WERA measurements of 9-min duration were made every 20 min, alternately by both stations. The distance between the two WERA sites was 10 km.

Unfortunately, a bottom-mounted acoustic Doppler current profiler (ADCP) did not work properly. For this reason, comparison of HF with *in situ* data is only possible with measurements of a S4 current meter which was deployed at the sea floor at a

TABLE IV
MEASUREMENTS DURING THE SCAWVEX PETTEN EXPERIMENT

site	parameter	sensor	period
P1	radial current	WERA	29 Oct - 5 Dec
P2	radial current	WERA	29 Oct - 5 Dec
MC	current vector	S4	11 Nov - 16 Dec
MD	wave spectra	waverider	1 Nov - 16 Dec
MW	wind vector	windsensor	1 Oct - 31 Dec

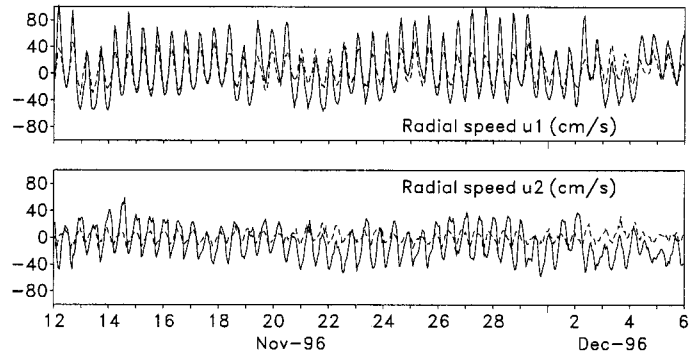


Fig. 10. Radial current speeds at position PC in Fig. 4 relative to the radar sites P1 and P2. Solid lines: measured by WERA at the sea surface. Dashed lines: measured by an S4 electromagnetic current meter mounted on the sea floor at 22 m depth.

depth of 22 m. Fig. 10 presents the results. The rms differences for both components are $23 \text{ cm}\cdot\text{s}^{-1}$. In general, the *in situ* velocities at the sea floor are smaller than the HF-measured velocities at the sea surface. This can be explained by friction processes at the sea bottom and by wind driven currents at the surface.

Similar to Fig. 9, Fig. 11 displays the waveheight, theoretically predicted and measured WERA standard deviation, and the estimated error. However, the determination of the measured standard deviation is somewhat different. It is orientated toward the peak frequency (or radial velocity) of the Doppler spectrum. The standard deviation is estimated from an interval around this peak which is $\pm 130 \text{ cm}\cdot\text{s}^{-1}$. The correlations between the waveheight component (top panel of Fig. 11) and standard deviation (third panel of Fig. 11) are high for both stations M1 and M2, $r = 0.79$ and $r = 0.89$, respectively. As compared to the CODAR measurements of Fig. 9, the waveheight shows more temporal variability.

Beamforming with WERA allows one to separate second-order side bands which are clearly visible in the Doppler spectra, cf. Fig. 3. The distance of the second-order peaks from the Bragg lines depends on the long wave spectrum and becomes smaller with increasing long wavelengths. In the case of the spectrum of Fig. 8, this distance is only $45 \text{ cm}\cdot\text{s}^{-1}$. Thus, the standard deviations in Fig. 11 contain contributions from second-order side bands. Again, the theoretical standard deviations are higher than the measured ones. But as compared to CODAR, the deviations are somewhat smaller.

V. SUMMARY AND CONCLUSIONS

Surface-current measurements of two HF radar systems, CODAR and WERA, are investigated. Both systems operate at

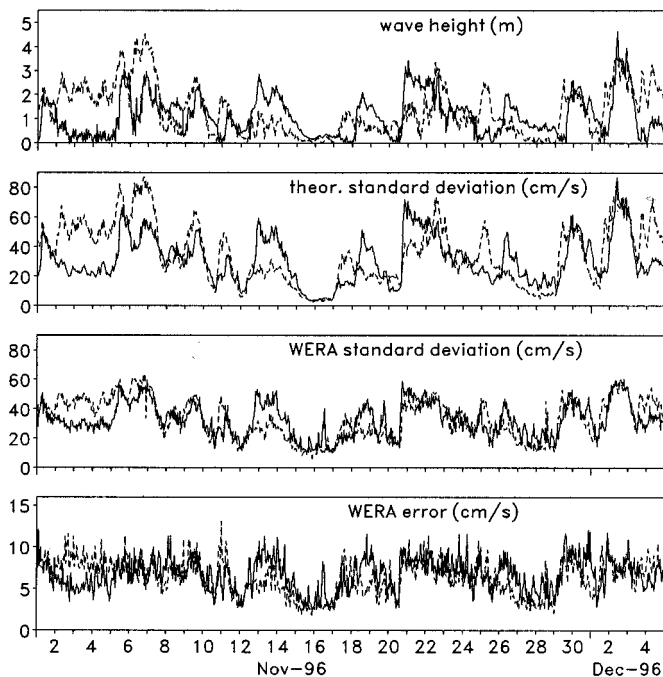


Fig. 11. Top panel: significant waveheight measured at PD in Fig. 4, parallel to the directions toward P1 (full line) and P2 (dashed line). Second panel: theoretically predicted standard deviations for the radial speeds of stations P1 (full lines) and P2 (dashed line). Third panel: standard deviations measured by WERA stations P1 (full line) and P2 (dashed line) at position PD. Bottom panel: WERA error derived from the standard deviation.

about 30 MHz, i.e., Bragg scattering is due to surface wavelengths of 5 m. HF-measured current velocities are compared with *in situ* measurements. Standard deviations are estimated from the Doppler spectra of the backscattered signal and analyzed with respect to their dependence on the sea state.

In accordance with results reported in the literature (cf. [11], [15]), the comparison of HF and an *in situ* measured current velocities reveals rms differences between 10 and 20 $\text{cm}\cdot\text{s}^{-1}$. High deviations occur occasionally with deviating tidal amplitudes or a phase shift between the tides. These events are independent of sea state. We suspect that some of the deviations are due to the different spatial averaging performed by the systems, i.e., to horizontally inhomogeneous currents or strong vertical current shear which are caused by the Rhine outflow.

First-order Bragg theory predicts the Doppler spectrum to consist of two discrete lines. The presence of long ocean waves causes a broadening of the spectrum due to: 1) second-order scattering and 2) wave orbital motion. The azimuthal resolution technique applied by CODAR (direction finding) is not able to separate both effects. Beamforming, as applied by WERA, reveals clearly visible second-order side bands in the Doppler spectra. However, these side bands overlap with the broadening of the Bragg lines due to the orbital motion of the long waves.

Standard deviations of the measured current speeds reveal a strong dependence on the sea state for both the CODAR and the WERA. The observed standard deviations are smaller than predicted by the composite wave model, although they additionally account for contributions from second-order side bands. The reduced standard deviation is partly due to the weighted averaging performed. Another reason for the discrepancy may

be that the requirements of the composite surface are partially violated. Errors in the HF measurements, as estimated from the standard deviations, range between 3 and 10 $\text{cm}\cdot\text{s}^{-1}$. This is in accordance with the comparison of CODAR and WERA measurements at a position 22 km offshore. The comparison of CODAR and WERA with the S4 electromagnetic current meter at the same position reveals rms differences of 15 $\text{cm}\cdot\text{s}^{-1}$ and 12 $\text{cm}\cdot\text{s}^{-1}$, respectively. It has been found that the WERA is more robust against disturbances like radio noise and ship traffic. For high sea states, no simultaneous measurements of CODAR and WERA are available. However, the investigation of the Doppler spectra shows (cf. Figs. 2 and 3) that the WERA allows a more accurate determination of the peak frequency and in turn of the current speed.

The investigations presented refer to the radial speeds measured by HF radar. By constructing 2-D vectors from the radial speeds, another error source arises from geometry, cf. [15]. If the angles between the radial components deviate from perpendicular, the error of at least one component exceeds those of the radial speeds.

ACKNOWLEDGMENT

The authors would like to thank their colleagues G. Antonis-chki, M. Hamann, and F. Schirmer, who participated in the HF experiments.

REFERENCES

- [1] D. D. Crombie, "Doppler spectrum of sea echo at 13.56 Mc/s," *Nature*, vol. 175, pp. 681–682, 1955.
- [2] D. E. Barrick, M. W. Evans, and B. L. Weber, "Ocean surface current mapped by radar," *Science*, vol. 198, pp. 138–144, 1977.
- [3] D. Prandl, S. G. Loch, and R. Player, "Tidal flow through the Straits of Dover," *J. Phys. Oceanogr.*, vol. 23, pp. 23–37, 1992.
- [4] K.-W. Gurgel, H.-H. Essen, and F. Schirmer, "CODAR in Germany – A status report valid November 1985," *IEEE J. Oceanic Eng.*, vol. OE-11, pp. 251–257, 1986.
- [5] J. D. Paduan and L. K. Rosenfeld, "Remotely sensed surface currents in Monterey Bay from shore-based HF radar," *J. Geophys. Res.*, vol. 101, pp. 20 669–20 686, 1996.
- [6] R. H. Khan and D. K. Mitchell, "Waveform analysis for high-frequency FMICW radar," *Geophys. Res. Lett.*, vol. 17, pp. 1097–1100, 1991.
- [7] E. D. R. Shearman and M. D. Moorhead, "PISCES, a coastal ground-wave HF radar for current, wind and wave mapping to 200 km ranges," *IGARSS'88 Proc.*, pp. 773–776, 1988.
- [8] P. Broche, J. C. Crochet, J. L. de Maistre, and P. Forget, "VHF radar for ocean surface current and sea state remote sensing," *Radio Science*, vol. 22, pp. 69–75, 1987.
- [9] M. L. Heron, "Directional spreading of short wavelength fetch-limited wind waves," *J. Phys. Oceanogr.*, vol. 17, pp. 281–285, 1987.
- [10] Y. Hisaki, "Nonlinear inversion of the integral equation to estimate ocean wave spectra from HF radar," *Radio Science*, vol. 31, pp. 25–39, 1996.
- [11] C. C. Teague, J. F. Vesecky, and Z. R. Hallock, "A comparison of multifrequency HF radar and ADCP measurements of near-surface currents during COPE-3," *IEEE J. Oceanic Eng.*, to be published.
- [12] K.-W. Gurgel, H.-H. Essen, and S. P. Kingsley, "High-frequency radars: Physical limitations and recent developments," *Coastal Eng.*, vol. 37, pp. 201–218, 1999.
- [13] H.-H. Essen, "Geostrophic surface currents as derived from satellite SST images and measured by a land-based HF radar," *Int. J. Remote Sensing*, vol. 16, pp. 239–256, 1995.
- [14] H. C. Graber, D. R. Thompson, and R. E. Carande, "Ocean surface features and currents measured with synthetic aperture radar interferometry and HF radar," *J. Geophys. Res.*, vol. 101, pp. 25 813–25 832, 1996.
- [15] H. C. Graber, B. K. Haus, R. D. Chapman, and L. K. Shay, "HF radar comparisons with moored estimates of current speed and direction: Expected differences and implications," *J. Geophys. Res.*, vol. 102, pp. 18 749–18 766, 1997.

- [16] H.-H. Essen, "Ekman portions of surface currents, as measured by radar in different areas," *Dt. Hydrogr. Z.*, vol. 45, pp. 58–85, 1993.
- [17] K. Hasselmann, "Determination of ocean wave spectra from Doppler radio return from the sea surface," *Nature*, vol. 229, pp. 16–17, 1971.
- [18] L. R. Wyatt, "HF radar measurements of the ocean wave directional spectrum," *IEEE J. Oceanic Eng.*, vol. 16, pp. 163–169, 1991.
- [19] J. W. Wright, "Detection of ocean waves by microwave radar; the modulation of short gravity-capillary waves," *Boundary-Layer Met.*, vol. 13, pp. 87–105, 1978.
- [20] W. J. Pierson and L. Moskowitz, "A proposed spectral form for fully developed wind seas based on the similarity theory of S.A. Kitaigorodskii," *J. Geophys. Res.*, vol. 69, pp. 5181–5190, 1964.
- [21] K. Hasselmann, T. P. Barnett, E. Bouws, H. Carlson, D. E. Cartwright, K. Enke, J. A. Ewing, H. Gienapp, D. E. Hasselmann, P. Kruseman, A. Meerburg, P. Müller, D. E. Olbers, K. Richter, W. Sell, and H. Walden, "Measurement of wind-wave growth and swell decay during the Joint North Sea Wave Project (JONSWAP)," *Ergänzungsheft zur Dt. Hydrogr. Z.*, no. 12, 1973.
- [22] B. Kinsman, *Wind Waves, Their Generation and Propagation on the Ocean Surface*. Englewood Cliffs, NJ: Prentice-Hall, 1965.
- [23] H.-H. Essen, K.-W. Gurgel, and F. Schirmer, "Surface currents in the Norwegian Channel measured by radar in March 1985," *Tellus*, vol. 41A, pp. 162–174.
- [24] —, "Horizontal variability of surface currents in the Dead Sea," *Oceanologica Acta*, vol. 18, pp. 455–467, 1995.
- [25] K.-W. Gurgel and H.-H. Essen, "On the performance of a ship-borne current mapping HF radar," *IEEE J. Oceanic Eng.*, vol. 25, pp. 183–191, 2000.
- [26] K.-W. Gurgel, G. Antonischki, H.-H. Essen, and T. Schlick, "Wellen Radar (WERA), a new ground-wave based radar for ocean remote sensing," *Coastal Eng.*, vol. 37, pp. 219–234, 1999.
- [27] P. K. Kundu, "Ekman veering observed near the ocean bottom," *J. Phys. Ocean.*, vol. 6, pp. 238–241, 1976.

Heinz-Hermann Essen received the diploma in physics and the Ph.D. degree in physics from the University of Hamburg (UH), Hamburg, Germany, in 1969 and 1976, respectively.

Until 1980, he worked at the UH Geophysical Institute in the fields of seismic and underwater acoustics. In 1981, he joined the UH Institute of Oceanography and started his work on HF remote sensing of the ocean. From 1991 until 1996, he was responsible for satellite remote sensing activities at the Saclant Undersea Research Center, La Spezia, Italy. His present research interests are in HF remote sensing, microwave wind scatterometry, and microseisms.

Klaus-Werner Gurgel (M'94) received the diploma in electrical engineering from the University of Hannover, Hannover, Germany in 1980 and the Ph.D. degree from the University of Hamburg (UH), Hamburg, Germany, in 1993.

From 1980 to 1985, he was responsible for the technical development and operation of UH's CODAR. In 1985, he started working on a shipborne version of the CODAR which was completed in 1993. In 1996, he developed the new HF radar WERA (Wellen RADar).

Thomas Schlick received the diploma in applied and neuronal physics from the University of Marburg, Marburg, Germany, in 1986.

After joining the remote sensing group at the Institute of Oceanography of the University of Hamburg, Hamburg, Germany, in 1986, he participated in the operation of UH's CODAR, and in the development and operation of WERA (Wellen RADar). Up to now, he was involved in various marine and remote sensing projects.